Available online at www.sciencedirect.com
SCIENCE DIRECT
Journal of Catalysis 237 (2006) 152–161
JOURNAL OF CATALYSIS
www.elsevier.com/locate/jcat

Investigation of promoter effects of manganese oxide on carbon nanofiber-supported cobalt catalysts for Fischer–Tropsch synthesis

G.L. Bezemer [a], P.B. Radstake [a], U. Falke [b], H. Oosterbeek [c], H.P.C.E. Kuipers [c], A.J. van Dillen [a], K.P. de Jong [a,*]

[a] *Inorganic Chemistry and Catalysis Debye Institute, Utrecht University, Sorbonnelaan 16, 3584 CA Utrecht, The Netherlands*
[b] *UK SuperSTEM, Daresbury Laboratory, Daresbury WA4 4AD, United Kingdom*
[c] *Shell Global Solutions, PO Box 38000, 1030 BN Amsterdam, The Netherlands*

Received 17 August 2005; revised 24 October 2005; accepted 27 October 2005

Abstract

The effects of the addition of MnO were studied on a carbon nanofiber-supported cobalt catalyst. The starting sample, cobalt loading 9.5 wt% and 8% cobalt dispersion, was promoted by impregnation with small amounts of MnO (0.03, 0.1, 0.3, 0.6, and 1.1 wt%). XPS and STEM-EELS showed MnO to be associated with Co in both dried and reduced catalyst. In the drying step, MnO was deposited on the passivated cobalt particles, because of the tendency of both metals to form stable mixed compounds. After reduction, the MnO remained close to the cobalt particles, because the support material lacked sites with significant interaction with MnO. The promoter suppressed both the hydrogen chemisorption uptake and the cobalt reducibility even with the lowest MnO loading. At 1 bar, large improvements in the selectivity toward C_{5+} products (from 31 to 45 wt%) were found with MnO loadings of 0.3 wt% and higher. At 20 bar, the addition of only 0.03 wt% MnO improved the C_{5+} selectivity from 74 to 78 wt%, but larger amounts decreased the selectivity to 52 wt% at 1.1 wt% MnO. The surface-specific activity (TOF) first increased with MnO loading from 26 to 60 $\times$ 10^{-3} s^{-1} for 0.3 wt% MnO, whereas it decreased, probably as a consequence of excessive Co surface coverage at MnO loadings >0.3 wt%. Product analysis (paraffin:olefin ratio) indicates that a major role of MnO involves moderation of hydrogenation reactions.

Keywords: Catalysts; CNF; Cobalt; Manganese; Promoter; STEM-EELS; XPS

1. Introduction

In the Fischer–Tropsch (FT) reaction synthesis gas (CO/H_2) is catalytically converted into hydrocarbons via surface polymerisation. Using synthesis gas produced from natural gas, coal, or biomass, transportation fuels can be produced from feedstocks other than crude oil. The quality of the products formed in combination with a non-crude oil feedstock support the FT process to play a crucial role in the worldwide energy supply in the coming decades.

Supported cobalt catalysts are well known for their activity and selectivity in the FT reaction [1]. The catalysts are often promoted with small amounts of noble metals to decrease the reduction temperature and increase the activity [2–4]. To achieve better selectivities toward long-chain products, special metal oxides can be added [4–7]. In this paper we investigate the influence of manganese oxide on cobalt supported on carbon nanofiber (CNF) catalysts. MnO is reported to be a promoter for cobalt-based FT catalysts in both academic and patent literature. Originally most research was devoted to cobalt on MnO_2 supports and to systems with mixed oxides of cobalt and manganese [8–12]. All of these systems have relatively high manganese loading. MnO promoter effects on cobalt catalysts supported on oxidic carriers were investigated recently [13–20]. The promoting effect of MnO is suggested to originate from a lower degree of cobalt reduction [12,13,20]. In all cases, a metal oxide was also used as support material, also decreasing cobalt reducibility and thus complicating the analysis. Therefore, we decided to reduce support effects by using an inert carrier, CNF. CNF is a novel graphitic support material with promising ap-

* Corresponding author. Fax: +31 30 2511027.
E-mail address: k.p.dejong@chem.uu.nl (K.P. de Jong).

0021-9517/$ – see front matter
doi:10.1016/j.jcat.2005.10.031

plications, including use as a support for FT catalysts [21,22]. Recently, we showed, using X-ray photoelectron spectroscopy (XPS) and STEM-EELS, that in Co/CNF catalysts promoted with MnO, the promoter is present only in the vicinity of the cobalt particles and not elsewhere on the support [23].

This paper provides a comprehensive characterization and systematic investigation at low and high pressure of the catalytic effects of manganese loading on Co/CNF catalysts. Catalysts with Co/Mn molar ratios varying from 11 to 431 were prepared and were characterized by acid–base titration, H_2 chemisorption, scanning transmission electron microscopy–electron energy loss spectroscopy (STEM-EELS), transmission electron microscopy (TEM), temperature-programmed reduction (TPR), XPS, and X-ray diffraction (XRD), whereas FT catalysis experiments were carried out in fixed-bed reactors at both atmospheric pressure and 20 bar.

2. Experimental

2.1. Catalyst preparation

CNF of the fishbone type (average diameter, ca. 30 nm) were grown from syngas as described previously [24]. After purification by refluxing in 1 M KOH, adsorption sites were created by refluxing the CNF in concentrated HNO_3, as described by Toebes et al. [25]. After washing and drying at 120 °C, CNF with a BET surface area of 160 m^2/g and a bulk density of 0.50 g/ml were obtained.

Cobalt was loaded on the activated CNF by incipient wetness impregnation (pore volume, 0.56 ml/g of a solution containing 0.97 g/ml $Co(NO_3)_2{\cdot}6H_2O$, resulting in a loading of 9.5 wt% cobalt in the final catalyst. The catalyst precursor was dried in air at 120 °C for 18 h and subsequently reduced at 350 °C for 2 h in a flow of 10% H_2/He. After passivation in a 1 vol‰ oxygen flow at room temperature, the sample, coded Co/CNF, was obtained.

Subsequently, manganese was loaded on six portions of Co/CNF using incipient wetness impregnation with aqueous solutions of $Mn(NO_3)_2{\cdot}4H_2O$ with different concentrations. A reference sample, coded CoH, was prepared by impregnation with a diluted HNO_3 solution (pH 5) to reveal any effects caused by the new preparation step. The catalysts loaded with manganese were coded Co431Mn, Co95Mn, Co39Mn, Co19Mn, and Co11Mn, the numbers indicating the respective cobalt to manganese atomic ratio (Table 1). All catalyst precursors were dried in air at 120 °C for 18 h.

2.2. Catalyst characterization

The number of acidic groups available before loading the support with cobalt or manganese was determined by titration [25]. The 50-mg treated and untreated CNF samples were suspended in a 25-ml solution of 0.1 M NaCl and 0.1 M oxalic acid in demi-water (pH = 3.0). Under continuous stirring, 10 mM NaOH was added dropwise at a rate of 0.05 ml/min until the final pH of 10 was reached. During the titration, the pH was monitored with a pH electrode. The difference between the amount of NaOH needed to reach pH 7 with the blank and with the sample is reported in mmol/g.

Table 1
Composition, H_2 uptake and calculated cobalt dispersion of the samples under investigation

Sample	Co (wt%)	MnO (wt%)	H_2 uptake (mmol/g)	Dispersion (%)
CoH	9.5	–	0.063	7.8
Co431Mn	9.5	0.028	0.063	7.8
Co95Mn	9.5	0.13	0.054	6.7
Co39Mn	9.5	0.30	0.051	6.4
Co19Mn	9.5	0.63	0.053	6.6
Co11Mn	9.4	1.1	0.052	6.5

Powder XRD patterns were measured using an Enraf-Nonius CPS 120 powder diffraction apparatus with Co-K_α radiation ($\lambda = 1.789$ Å). Temperature-programmed reduction was executed with an Autochem 2920 instrument from Micromeritics. Typically 0.1 g sample was after drying reduced in a flow of 50 ml/min 5% H_2/Ar, the temperature was increased with 5 °C/min from room temperature to 750 °C.

XPS measurements were performed on a Thermo VG Scientific XPS system using non-monochromatic Mg (K_α) radiation. The XPS apparatus was equipped with a reaction chamber in which samples could be reduced in situ. The CoH and Co11Mn samples were measured both after drying and after in situ reduction at 350 °C for 2 h; the other samples were measured only after drying. The pass energy of the analyser was set at 70 eV. Charging effects were minimal, with shifts of at most 0.2 eV. The C peak at 284.2 eV was used as a reference, to correct for the charging of the samples. The escape depth of the photoelectrons generated is small (∼1.5 nm), which, if the surface area of the support and metal loading are known, allows evaluation of particle size. Particle sizes for cobalt and manganese oxide have been calculated from the quantitative Co/C and Mn/C ratios using the model for hemispherical particle shapes [26–28].

Hydrogen chemisorption measurements were carried out with a Micromeritics ASAP 2010C. Before each measurement, the sample was dried in vacuum at 120 °C overnight and reduced for 2 h in flowing H_2 at 350 °C at a heating rate of 5 °C/min. After reduction, the samples were evacuated at that temperature for 30 min. The H_2-adsorption isotherms were measured at 150 °C, as recommended by Reuel and Bartholomew [29]. The H/Co ratios at zero pressure were found by extrapolating the linear part of the isotherm. Calculations were made using the total amount of hydrogen adsorbed assuming complete reduction and a stoichiometry of 1 hydrogen atom per cobalt surface atom [29].

The dried catalyst precursors and the reduced catalysts were examined by TEM (FEI Tecnai12 operating at 120 kV, or FEI Technai20F operating at 200 kV). Samples were crushed and subsequently suspended in ethanol under ultrasonic vibration. A drop of this suspension was loaded onto a holey carbon film on a copper grid.

The sample with the highest manganese loading was examined in a dedicated aberration-corrected STEM (VG HB501),

equipped with a Nion Mark II C_s corrector and a Gatan Enfina spectrometer to obtain EELS spectra. High-angle annular dark field (HAADF) images were acquired at an acceptance angle of 70–210 mrad. The acquisition time for a full image was around 45 min. In total, we measured 14 full images and 8 line-scans, each taken on different parts of the specimen.

2.3. Catalytic testing

Catalysts were tested at atmospheric pressure and at high pressure. The measurements at 1 bar were carried out at 220 °C using CO/H_2 (1/2 v/v) after a reduction treatment at 350 °C for 2 h in hydrogen flow. Typically, 30 mg of catalyst particles (0.5–1.0 mm) was diluted with 200 mg of SiC particles (0.2 mm) to achieve isothermal plug flow conditions. Selectivities of the catalysts were established at a CO conversion of 2%, which was achieved by tailoring the space velocity. For the high-pressure measurements, 0.25 g of catalyst (150–212 μm) was diluted with 0.5–0.7 g SiC. Catalysts were also reduced in hydrogen at 350 °C for 2 h, and the catalytic data were obtained at 220 °C and a pressure of 20 bar using a flow of $CO/H_2/N_2$ (33/66/6). The space velocity was adjusted to maximise CO conversion at around 60%. Reported catalytic data were obtained after 3 days of operation. Values for catalyst deactivation were based on the decrease of activity from day 1 to day 3 and are reported as percentage of activity per day.

3. Results and discussion

3.1. Titration

The activated CNF used for loading Co contained 0.15 mmol of acidic groups per gram. MnO was loaded on the Co/CNF after a reduction treatment at 350 °C for 2 h. Unfortunately, the amount of acidic groups on Co/CNF could not be measured directly, because the presence of cobalt interfered. Therefore, a sample of the original oxidised, unloaded CNF batch was reduced in H_2 at 350 °C and subsequently titrated. This sample contained only 0.06 mmol/g, which is an upper limit for the acid sites in Co/CNF that can serve as anchoring groups for the manganese. Despite this decrease in acidic surface groups, however, we noticed that the CNF were still hydrophilic, because wetting by water occurred smoothly.

3.2. XRD

XRD patterns of the unpromoted reduced and passivated Co/CNF together with dried CoH and dried Co11Mn are shown in Fig. 1. The starting material Co/CNF exhibits graphite diffraction lines, as well as contributions from CoO and metallic Co. The graphite diffraction lines are present at 30°, 51°, 63°, and 95° 2θ, whereas the diffractions at 43° and 77° 2θ are indicative for CoO. Line-broadening analysis of the 43° 2θ diffraction resulted in a domain size of 3 nm for CoO. The main diffraction line for metallic cobalt is present at 52° 2θ and coincides with graphite contributions, and three more metallic lines are found at 61°, 91°, and 114° 2θ, characteristic of fcc cobalt. Although hcp is the most stable structure for bulk cobalt, up to the transition temperature of 416 °C, small cobalt particles are reported to have the fcc structure [29,30]. The presence of CoO domains of 3 nm together with metallic Co in the sample demonstrates that reoxidation during the passivation treatment was not complete but probably resulted in the formation of a shell of cobalt oxide surrounding a metallic core.

The dried CoH and Co11Mn as a representative example of the CoMn/CNF catalysts showed distinct diffractions typical for Co_3O_4. No diffraction lines other than those of CNF or Co_3O_4 were observed. Apparently, cobalt originally present in Co/CNF as CoO and Co metal was oxidised to Co_3O_4 during impregnation and drying. The formation of Co_3O_4 was also observed in the dried MnO-promoted samples. For Co11Mn, no additional diffractions originating from manganese compounds were observed, probably because the manganese loading was too small (Fig. 1).

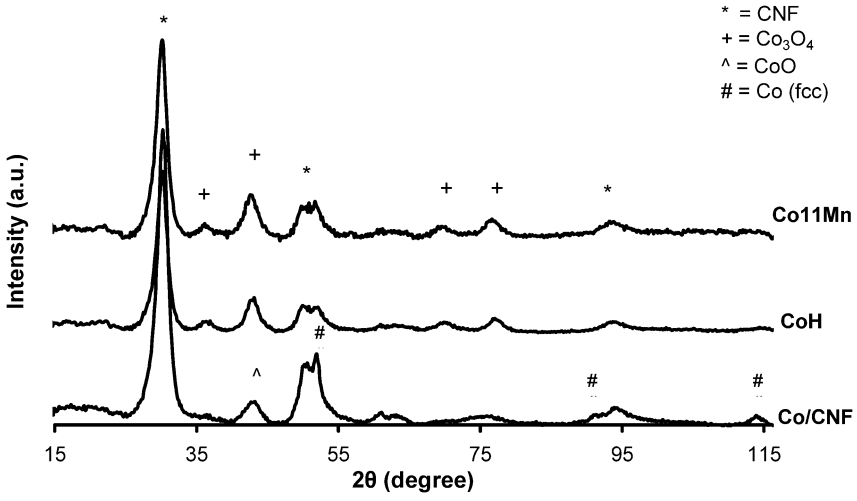

Fig. 1. XRD patterns of original reduced and passivated Co/CNF together with the dried samples CoH and Co11Mn with strongest diffraction lines of main components indicated.

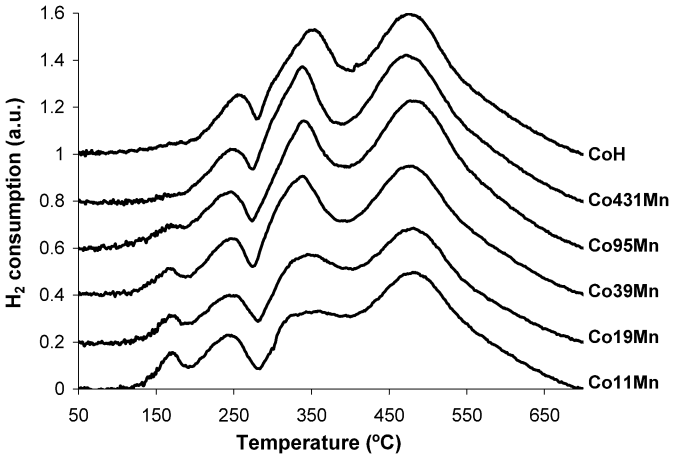

Fig. 2. TPR profiles of the dried samples, normalised on cobalt intake.

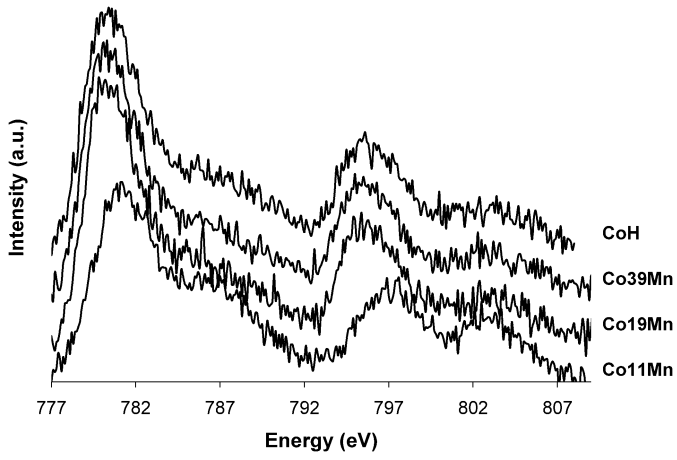

Fig. 3. Co 2p XPS region of dried CoH and the three catalysts with highest MnO loading. Spectra have been normalized to carbon 1s.

3.3. TPR

TPR profiles of the dried samples given in Fig. 2 show four distinct reduction peaks around 175, 240, 340, and 475 °C. The first peak at 175 °C, which increases with increasing manganese loading, can be ascribed to reduction and decomposition of nitrates [29]. The peak area of the second peak at 240 °C is unaffected by manganese loading. This peak stems from the reduction of Co^{3+} to Co^{2+}, showing that Co_3O_4 is present in the dried catalyst precursors, as was found with XRD. We used peak fitting to get an estimation of the peak areas of the Co^{3+} reduction peak at 240 °C and the Co^{2+} reduction peak at 340 °C in CoH. From the ratio of the peaks, it can be concluded that indeed all cobalt in the dried samples is present as Co_3O_4.

Interestingly, the Co^{2+} to Co^0 reduction found at 340 °C is influenced by the presence of MnO. CoH and the catalysts with MnO loading up to 0.30 wt% MnO have similar peak areas, but with higher manganese loadings, the intensity of the peak for the CoO to Co reduction decreases, indicating a strong interaction between CoO and MnO. The run-up of the broad peak around 475 °C makes quantitative identification difficult, but assuming similar peak shapes with peak fitting, we obtained peak area ratios higher than 1:3 for CoH and the three catalysts with the lowest manganese loadings, suggesting complete reduction. However, the samples with higher manganese loading have a broadened reduction peak, making quantitative analysis impossible. Taking into account the shift of the CoO reduction peak to higher temperatures, it is possible that some cobalt will remain unreduced after the reduction treatment (350 °C, 2 h) before H_2 chemisorption, in situ XPS, and catalytic testing.

The last broad reduction peak with a maximum around 475 °C could be ascribed to some gasification of CNF to methane, as GC analysis demonstrated. The higher the manganese loading on the catalysts, the lower the gasification peak. The TPR pattern of the support (data not shown) has a support reduction peak around 600 °C, indicating that metallic cobalt acts as a catalyst, probably through the spillover of hydrogen atoms. Now from Fig. 2 it can be concluded that adding manganese to the catalyst lowers the gasification peak area, indicating that either cobalt does not reduce completely at 475 °C (which is rather unlikely) or that MnO remains associated with the metallic cobalt particles, thus reducing the cobalt surface area available for catalytic gasification of carbon.

Table 2
Atomic ratios of four dried catalysts as obtained with XPS

Sample	Co/C	Mn/Co	Mn/C
CoH	0.022	–	–
Co39Mn	0.020	0.08	0.0017
Co19Mn	0.021	0.16	0.0036
Co11Mn	0.018	0.32	0.0059

3.4. XPS

Fig. 3 shows the Co 2p spectra normalised on the carbon 1s peak area for the dried CoH and the three catalysts with the highest manganese loadings: Co39Mn, Co19Mn, and Co11Mn. Distinct peaks stemming from $2p_{3/2}$ at 780.0 eV and $2p_{1/2}$ at 795.4 eV can be seen for CoH, characteristic of Co_3O_4. For the sample with the highest Mn loading, Co11Mn, both peaks are shifted to significantly higher binding energies, 780.9 and 797.2 eV, indicating the presence of a different cobalt compound at the surface of the cobalt particles. The mixed spinel of cobalt and manganese oxide and CoO have binding energies similar to the observed values [31]. In Co19Mn and Co39Mn, some broadening of the cobalt peak is observed, but a distinct shift to higher binding energy as with Co11Mn is not observed, which might be explained by the lower Mn loadings that were insufficient to lead to mixed spinel formation.

Table 2 gives the Co/C, Mn/Co, and Mn/C atomic ratios as measured by XPS. The cobalt particle size in CoH was calculated from the Co/C ratio as 11 nm. The loading of MnO on the samples resulted in a small but distinct lowering of the Co/C atomic ratio, as found previously [23]. The atomic ratio of Co/C decreased from 0.022 to 0.018 going from CoH to Co11Mn (Table 2). This decrease in Co/C could be explained if the cobalt particle size increased from 11 to 15 nm going from CoH to Co11Mn. But our TEM analysis did not find any indication of larger cobalt particle sizes related to the presence

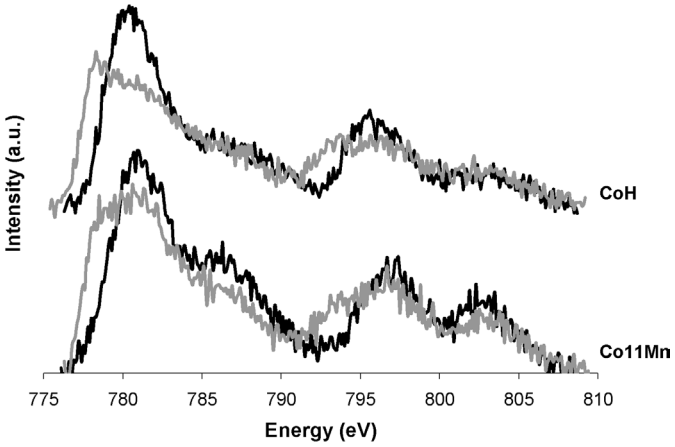

Fig. 4. Co 2p XPS region before (black) and after reduction (grey) for CoH and Co11Mn, spectra have been normalized to carbon 1s.

of MnO. An alternative explanation would be the coverage of cobalt(oxide) by MnO. From the STEM-EELS measurements (vide infra) we found that manganese and cobalt are superpositioned. The mean escape depth of the photoelectrons generated through MnO is only 1.2 nm, implying that the coverage of cobalt(oxide) by small amounts of MnO can significantly reduce the amount of photoelectrons reaching the detector. Consequently, the present decrease in Co/C ratio can be very well explained by coverage of the cobalt oxide particles with MnO.

The Mn/C atomic ratios obtained from XPS (Table 2) were more than three times higher than the overall Mn/C ratio, demonstrating that MnO is highly dispersed on the samples. For Co11Mn, we obtained from XPS a MnO particle size of 0.6 nm assuming a hemispherical shape or 0.4 nm for spherical particles. XPS is not able to discriminate between these options, but nonetheless we can conclude from these data that MnO is highly dispersed in Co11Mn, and, as discussed above, most likely (partly) located on top of the cobalt(oxide) particles. For Co19Mn and Co39Mn, using the Mn/C ratios we found even smaller MnO particle sizes of 0.3–0.4 nm, demonstrating that the size of the MnO particles is affected by the loading.

The influence of manganese on the cobalt oxidation state after reduction was also investigated with XPS. The Co 2p spectra before and after reduction of CoH and Co11Mn are given in Fig. 4. For CoH, the Co 2p binding energies shifted from 780.0 and 795.4 eV in the dried sample to 778.2 and 793.5 eV in the reduced sample, values indicative of metallic cobalt. After reduction, a shoulder remained at the oxidic position showing that not all cobalt was reduced. For the promoted sample Co11Mn, the peak maximums did not shift after reduction, although significant shoulders at the metallic cobalt positions were formed. This shows that the outer layer of the cobalt particles in Co11Mn was mainly oxidic, whereas in CoH the majority of cobalt atoms probed were reduced. The higher oxidation state of cobalt due to the presence of MnO is in line with the TPR results, which showed a pronounced influence of MnO on cobalt reduction. The atomic ratios between Co, C, and Mn did not change on reduction, showing the absence of significant restructuring of the phases leading to changes in their dispersion. This makes it likely that Co and Mn remained closely associated after the reduction treatment.

3.5. H_2 chemisorption

The hydrogen uptake data and the calculated apparent dispersions of the catalysts are given in Table 1. It was not possible to obtain the actual degree of reduction of cobalt, because back-titration with oxygen interfered with the oxidation of the support material. Therefore, we assumed complete reduction, which, as mentioned in the discussion of the TPR patterns, might not be valid for the two samples with the highest MnO loadings. Consequently, the actual dispersion of these samples could be higher than the values reported. For the unpromoted sample CoH, we found a cobalt dispersion of 7.8%, corresponding to an average cobalt particle size of 12 nm [29], close to the result of 11 nm found with XPS. Adding 0.028 wt% MnO resulted in the same cobalt dispersion, but adding higher amounts of manganese lowered the cobalt dispersion to the lowest value, 6.4%. The presence of manganese oxide on the cobalt surface may decrease hydrogen chemisorption uptake in two different ways. The coverage of cobalt atoms at the surface by MnO decreases the amount of sites probed with chemisorption. It is also possible that MnO decreases the ultimate degree of reduction of cobalt, which also decreases the hydrogen uptake.

From Table 1, it is clear that the exposed cobalt surface as probed by hydrogen chemisorption did not decrease further for MnO loadings higher than 0.30 wt%. The particle size for MnO calculated from quantitative XPS for Co39Mn was 0.3–0.4 nm, about the height of a monolayer of MnO. Thus, for low MnO loadings we expect MnO to be present mainly as monolayer patches on the cobalt particles.

For higher MnO loadings, monolayer coverage of the cobalt surface by MnO is unlikely. It was calculated that the Mn loading of Co11Mn is equivalent to an MnO monolayer over the cobalt surface, which would block all of the sites present for hydrogen chemisorption. But the amount of H_2 chemisorbed was still 80% of that of the unpromoted catalyst, from which we can conclude that for this MnO loading, the promoter is not exclusively present as a monolayer on the cobalt metal. Quantitative XPS for Co11Mn exhibited MnO particle sizes of 0.4–0.6 nm, corresponding to approximately two times the thickness of a monolayer. Therefore, we propose that at higher MnO loadings, a significant part of MnO is located on the CNF surface in the close vicinity of the cobalt particles. The development of the MnO structure with increasing loading is depicted in Fig. 5.

3.6. TEM

TEM was used to measure the particle size distribution in the original reduced and passivated Co/CNF sample. The majority of the particles observed had sizes around 8 nm. Fig. 6 shows small cobalt(oxide) particles supported on the carbon nanofibers. The small particles display limited contrast with the graphite support, possibly indicating that they have been oxidised. Indeed, in the high-resolution image depicted in Fig. 7 the d-spacing (0.21 nm) points toward the presence of CoO. In

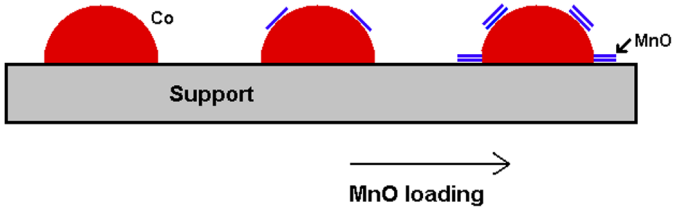

Fig. 5. Schematic representation of the location of MnO on the cobalt catalysts. Until Co39Mn we find MnO mainly present as monolayers on Co, for higher loadings MnO forms multi-layers and is also found on the CNF support, still in close contact with the Co particles.

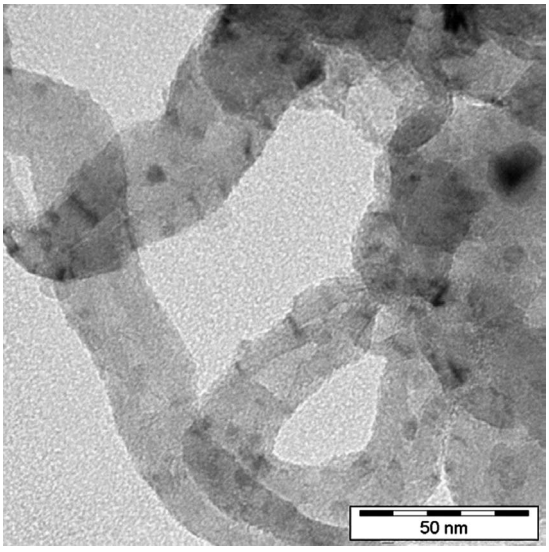

Fig. 6. TEM image of original Co/CNF catalyst showing the interwoven carbon nanofibers structure of the support with small supported cobalt particles with limited contrast.

addition, some larger particles (up to 25 nm) were present, thus shifting the average particle size toward the value (12 nm) obtained from H_2 chemisorption.

3.7. STEM-EELS

STEM-EELS was performed to gain more insight into the location of manganese and cobalt both before and after the reduction treatment. Toward this end, the sample with the highest manganese loading, Co11Mn, was studied. Fig. 8A shows a representative dark field image together with the areal densities of carbon, cobalt, manganese, and oxygen of the dried sample. In the dark field image, an individual carbon nanofiber is depicted on which several brighter spots are visible. By comparing the dark field image with the elemental mappings, it can be concluded that these brighter spots in dark field, with sizes varying from 4 to 14 nm, are composed of cobalt oxide and manganese oxide. Moreover, the elemental mappings and the bright field image shown in Fig. 8B suggest that the particles contain both metals; however, the 8-nm particle in the lower left corner does not appear in the manganese mapping. This indicates that although manganese is always associated with cobalt, the opposite is not true. Mixed particles prevailed; in total, we detected 54 Co–Mn particles and only 2 monometallic Co particles.

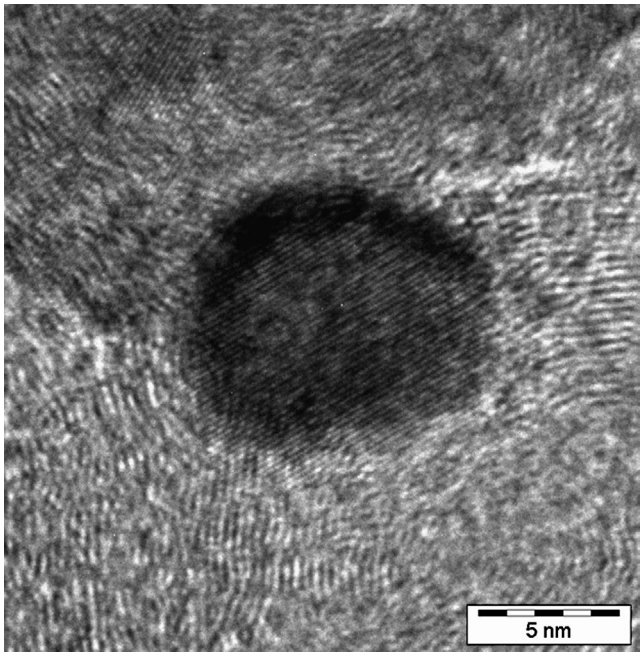

Fig. 7. HRTEM image of original Co/CNF sample with *d*-spacing typical for CoO.

The Mn patches have slightly different shapes than the Co patches, suggesting that Mn is covering Co, a conclusion that also could be drawn from the presented XPS data. This finding is also in line with literature results demonstrating that mixed oxides of cobalt and manganese are sometimes surface-enriched in manganese [32]. Moreover, this larger size for the MnO particles strongly suggests that part of the promoter is present on the CNF support, although closely associated with Co.

Fig. 9 shows the HAADF image and the elemental mappings with high resolution of two different single particles after reduction and passivation. The elemental mappings of cobalt, manganese, and oxygen shown Fig. 9A are correlated, and thus it can be concluded that cobalt, manganese, and oxygen remained associated after the reduction treatment. However, closer examination shows that cobalt matches the particles imaged by HAADF, whereas the manganese mapping is noncontinuous, pointing toward segregation on an atomic scale. Segregation is also seen in Fig. 9B, where the upper left part of the particle contains only cobalt oxide, whereas the other parts consist of both cobalt and manganese oxide. This indicates that during the reduction of cobalt oxide, MnO was partly redistributed over the cobalt metal surface. This finding agrees with the results of XPS and H_2 chemisorption indicating a free metallic Co surface next to MnO coverage.

3.8. Catalysis

The steady-state performance of the catalysts at 1 bar after 48 h is illustrated in Fig. 10 and characterised in Table 3. The presence of MnO influenced both the activity and the selectivity of the catalysts. On manganese loading, the C_{5+} selectivity increased from 31 to 45 wt%, mainly at the expense of methane

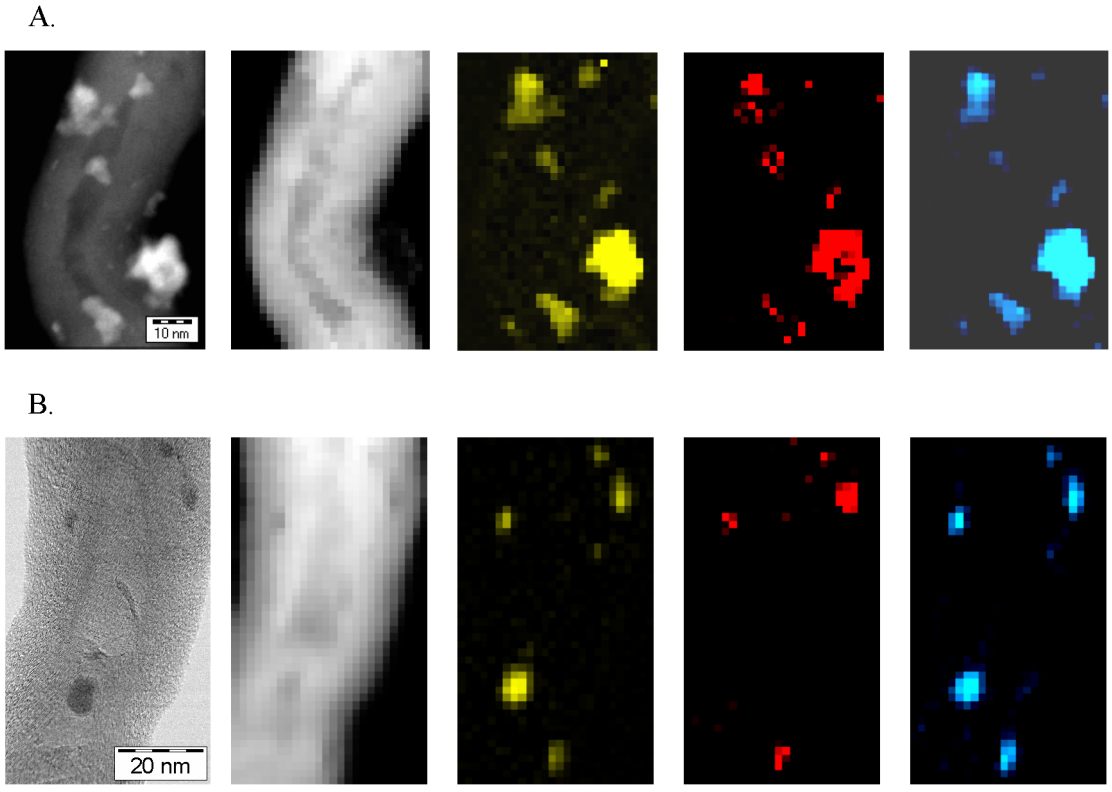

Fig. 8. STEM-EELS images of dried Co11Mn, from left to right: the HAADF (A) or bright field image (B) and the C, Co, Mn and O areal densities, derived from the EELS signals for two parts (A, B) of the specimen.

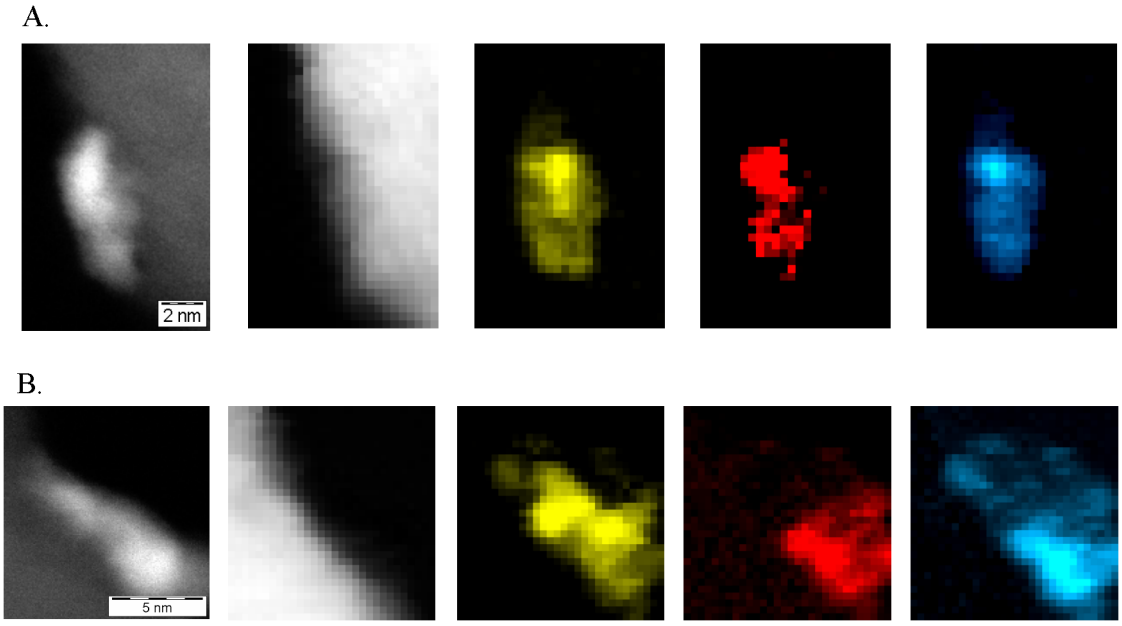

Fig. 9. STEM-EELS of reduced Co11Mn, from left to right: the HAADF image and the C, Co, Mn and O areal densities as derived from the EELS signals for two parts (A, B) of the specimen.

formation, which decreased from 36 to 23 wt%. We note that C_{5+} selectivity increased markedly up to Co39Mn, but did not improve further with higher Mn loadings. Fig. 11 plots the product distribution for CoH and Co11Mn. Clearly, the catalysts display ASF kinetics, and the chain growth probabilities can be derived from the linear part of the plot. An increase in alpha from 0.60 to 0.67 was found going from the unpromoted to the highest-loaded sample, with a similar trend as with the methane and C_{5+} selectivities.

The activity of the catalysts at 1 bar decreased on loading of MnO from 1.78 to 1.17×10^{-5} $\mathrm{mol_{CO}/(s\,g_{Co})}$, but the samples Co431Mn and Co95Mn showed no decrease in activity.

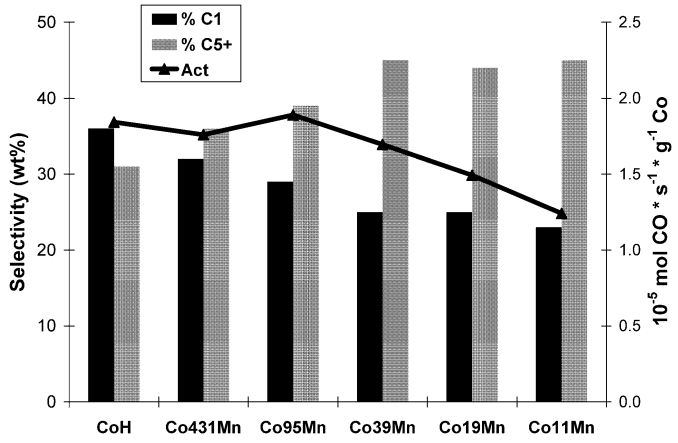

Fig. 10. Influence of manganese loading on activity and selectivity in the FT reaction at 1 bar.

Table 3
FTS catalytic performances at 1 bar, 220 °C[a]

Sample	Activity	TOF (10^{-3} s^{-1})	C_1 (wt%)	C_{5+} (wt%)	Alpha
CoH	1.8	14	36	31	0.60
Co431Mn	1.7	13	32	36	0.63
Co95Mn	1.8	17	28	41	0.65
Co39Mn	1.6	16	25	45	0.67
Co19Mn	1.4	13	25	44	0.66
Co11Mn	1.2	11	23	45	0.67

[a] Activity: 10^{-5} $mol_{CO}/(s\,g_{Co})$.

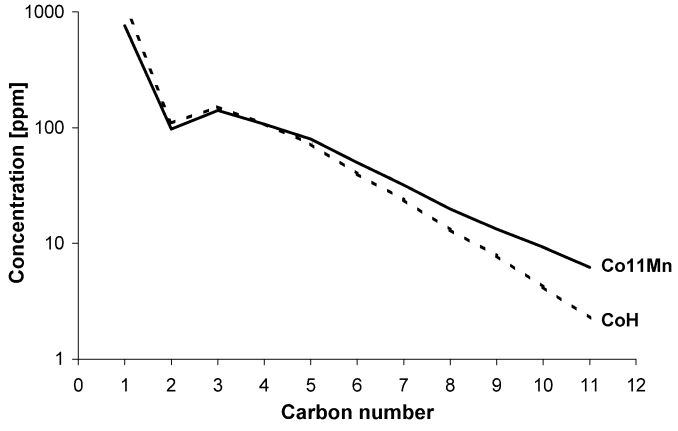

Fig. 11. ASF plot for CoH and Co11Mn showing the influence of MnO on the chain growth probability and the product distribution at 1 bar.

This demonstrates that small amounts of MnO on the catalyst improve the selectivity without hampering the activity. This is even more interesting because we found a decrease in the hydrogen chemisorption uptake for Co95Mn of 15% compared with the reference sample (CoH). The activity normalised on the cobalt surface area, the turnover frequency (TOF), increased from 14 to 17 $\times$ 10^{-3} s^{-1} going from CoH to Co95Mn. In addition, Co39Mn showed a higher TOF than the unpromoted sample. Therefore, minor amounts of MnO on the surface of cobalt result in higher TOF values for the remaining sites. But the TOF values mentioned are based on the exposed cobalt surface area in the reduced samples before the catalytic operation.

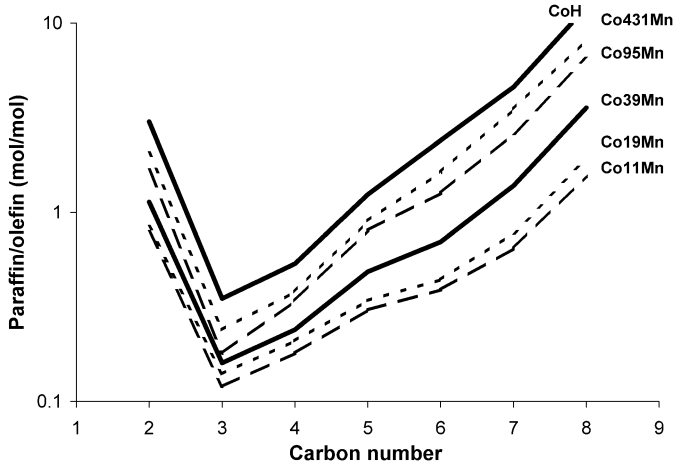

Fig. 12. Influence of manganese loading on the ratio between paraffins and 1-olefins in the products at 1 bar.

Because the actual cobalt catalyst is created in situ, the observed differences in TOF can also be related to changes to the catalyst under reaction conditions [33]. We could not measure the hydrogen chemisorption after catalytic operation, and thus we report these apparent TOF values.

Loading of more than 0.13 wt% MnO resulted in a decrease in activity. This decreased activity demonstrated the same trend as the decrease in dispersion obtained from H_2 chemisorption but was stronger. This resulted in a 35% lower TOF going from Co95Mn to Co11Mn. This clearly indicates that sites present for H_2 chemisorption are not one-to-one active for the FT reaction, but rather that ensembles of cobalt sites are needed for the FT reaction. This is comparable with our previous preliminary results on the cobalt particle size effect in FT catalysis, where cobalt particles smaller than 12 nm were less active for the FT reaction and exhibited far lower TOF values [22].

Another interesting feature of the MnO-promoted catalysts is the change from paraffin-rich to olefin-rich products. Fig. 12 shows the paraffin over olefin ratio for the linear products for carbon numbers 2 to 8. The P/O ratio at all carbon numbers systematically decreased with the MnO loadings on the samples. The impact of addition of only 0.03 wt% MnO is again pronounced, with a decrease of octane/octene ratio from 11 to 8. In the paraffin-to-olefin ratio, the trade-off between the primary hydrogenation activity and C–C coupling activity of the catalyst is manifested. As the hydrogenation activity of the catalysts decreases, more long-chain products are formed, as well as products that contain more olefins, which is the case for MnO-promoted catalysts. A main role of the MnO promoter at 1 bar is therefore suppression of the hydrogenation activity of the metallic cobalt.

Catalytic performances measured at 20 bar, a more relevant condition for industrial applications, are reported in Table 4. The loading of MnO on the catalysts influenced both the activity and the selectivity of the catalysts. The cobalt-specific activity increased from 4.1 to 6.8 $\times$ 10^{-5} $mol_{CO}/(s\,g_{Co})$ going from the unpromoted catalyst to Co95Mn. Adding higher amounts of MnO caused a rapid decrease in activity to 2.7 $\times$ 10^{-5} $mol_{CO}/(s\,g_{Co})$ for Co11Mn. The differences in the TOF,

Table 4
FTS catalytic performances at 20 bar, 220 °C[a]

Sample	Activity	Deact. (%/day)	TOF (10^{-3} s^{-1})	C_1 (wt%)	C_{5+} (wt%)	Alpha
CoH	4.1	7	26	18	74	0.91
Co431Mn	5.1	6	37	14	78	0.89
Co95Mn	6.8	3	60	15	77	0.89
Co39Mn	5.8	3	54	20	66	0.86
Co11Mn	2.7	7	25	21	52	0.85

[a] Activity: 10^{-5} $mol_{CO}/(s\,g_{Co})$.

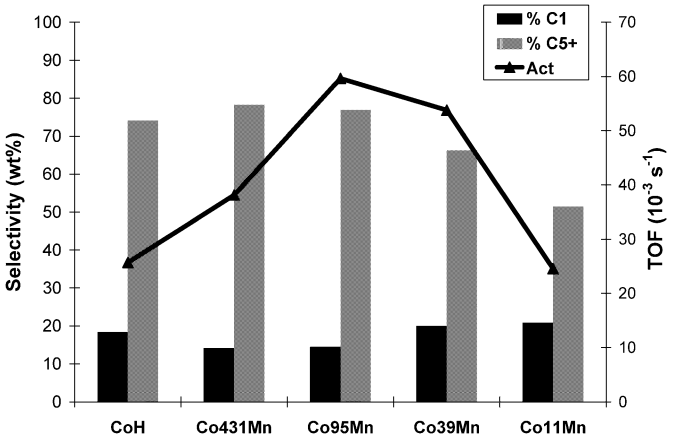

Fig. 13. Influence of manganese loading on activity and selectivity in the FT reaction at 20 bar.

also plotted in Fig. 13, were even larger and varied from 26 to 60×10^{-3} s^{-1} between CoH and Co95Mn. Interestingly, similar TOF values were found for the unpromoted catalyst and the overpromoted catalyst. The catalysts deactivated with 4–7% of their activity per day, values that gradually declined in time. Meanwhile, stable selectivities were found. The addition of small amounts of MnO was beneficial for catalyst stability. The relative periods of time on stream in this study do not allow firm conclusions on the influence of MnO on the stability of the catalysts.

The methane selectivity of the catalysts varied from 14 to 21 wt%. Adding only 0.03 wt% MnO resulted in a decrease in methane selectivity from 18 to 14 wt%, but adding higher amounts of MnO caused progressively higher methane selectivities up to 21 wt%. On manganese loading, the C_{5+} selectivity first increased from 74 to 78 wt% for Co431Mn before decreasing to 52 wt% for Co11Mn. Also at 20 bar, the promoted catalysts contained more olefins, whereas the chain growth probability decreased continuously on the addition of MnO from 0.91 to 0.85. It is known that the selectivity of catalysts in the FT can vary largely with reaction conditions [33,34]. However, the presented data were measured at the same conditions and similar CO conversions, enabling study of the influence of MnO as a promoter within this series.

Comparison of the catalytic data obtained at 1 bar and at 20 bar shows both similarities and large differences. At both conditions, the TOF increased on the loading of MnO; however, the 20% increase at 1 bar was modest compared with the 130% increase at 20 bar. From work on single crystals, it is known that metal oxides can increase the specific activity for CO hydrogenation and that addition of too large amounts of the promoting element causes a decrease in TOF [35,36], confirming the trend in our data. In addition, operating at high pressure, promoted catalysts can have higher turnover rates, with, for instance, a three-fold increase in TOF for Ru-promoted cobalt catalysts [37]. The greater influence of MnO on the specific activity at 20 bar could be related to the more severe conditions at high pressure. For example, the presence of MnO in combination with cobalt surface reconstruction might create more sites on the catalyst that are active in chain growth. However, more research is needed to verify this hypothesis.

The trends in chain growth probability were completely different: an increase from 0.60 to 0.67 at 1 bar versus a decrease from 0.91 to 0.85 at 20 bar. Related to these changes in chain growth probability was a clear optimum in C_{5+} selectivity at 20 bar, whereas it remained high at 1 bar, also at high MnO loadings. The influence of MnO loading on selectivity at 1 bar is most likely related to the initially very low C_{5+} selectivity due to the high hydrogen coverage on the catalyst surface [38]. Adding MnO may decrease the hydrogen coverage on the catalyst, hereby increasing the C_{5+} selectivity. For the 20 bar experiments, the catalyst surface is already largely covered with CO, resulting in a high C_{5+} selectivity even for the unpromoted catalyst. The role of the promoter is now more delicate, and overpromotion causes lower selectivity toward desired products [12].

3.9. Association of Mn with Co

The data presented so far show that small amounts of manganese have a significant influence on the cobalt reducibility and dispersion (TPR and H_2 chemisorption) and that MnO is present on the cobalt(oxide) particles in the dried and in the reduced samples (XPS and STEM-EELS). Now the question arises why manganese is only present associated with cobalt and is not located elsewhere on the CNF surface. Two explanations can be brought forward to answer the question. The first explanation addresses the number of available sites for anchoring the manganese during preparation; the second deals with the extent of interaction with sites on CoO and sites on carbon. From the titration experiment, we know that the reduction treatment of the support material diminishes the number of acidic groups to only 0.06 mmol per gram of sample. But the partly oxidised cobalt particles account for a three times higher amount of oxygen surface groups in the sample. Assuming similar occupancies, this would result in most of the manganese being located on top of the cobalt.

In the second explanation, the presence of manganese oxide on top of the cobalt oxide particles is explained by the greater interaction of MnO with CoO than with carbon. Co and Mn have similar ionic radii and readily form stable mixed oxides [32,39]. Because we did not detect any manganese located on the CNF support, an unexpected finding with an equal distribution over the support oxygen groups and the cobalt oxide (vide supra), the most likely reason for the presence of manganese on top of cobalt in the dried catalyst is the high extent of

interaction between cobalt and manganese oxide. However, during the reduction treatment the cobalt particles become metallic, diminishing the interaction with MnO. In their study on MnO promotion in Co/TiO_2 catalysts, Morales et al. observed the migration of MnO away from the cobalt to the support during the reduction step [19]. In our case MnO did not interact with the inert graphite surface (e.g., Mn carbides were not observed in XPS), thus favoring the presence of the promoter close to the cobalt particles. This is an important reason why CNF is a valuable support material for studying promoter effects in FT catalysis without interference of support effects.

4. Conclusion

In this paper we have shown that CNF provides a suitable support for studying the manganese promotion effect in cobalt-based FT catalysis, because it enables the study of a promoter effect without interference of support effects. Therefore, cobalt properties can be influenced by the addition of MnO loadings as low as 0.03 wt%. XPS and STEM-EELS demonstrated that manganese is closely associated with cobalt both in the catalyst precursor and in the final catalyst. We found that manganese retards cobalt reduction and, using in situ XPS, showed that the surface of the cobalt is more oxidic when MnO is added to the catalysts. Catalytic performance was affected differently in tests at 1 bar and at 20 bar. At 1 bar, the chain growth probability increased, and simultaneously the product distribution shifted toward olefinic products at increasing MnO loadings. This demonstrates that the presence of MnO moderates the hydrogenation activity of the catalysts. Interestingly, at 1 bar, the TOF increased by 20% on loading with small amounts of manganese (0.13 wt% MnO). In the experiments at 20 bar, C_{5+} selectivity first increased from 74 to 78 wt% at 0.03 wt% MnO before decreasing to 52 wt% for 1.1 wt% MnO. The TOF increased with at most 130% at 0.13 wt% MnO, clearly showing that this promoter can favorably affect both activity and selectivity, depending on concentration and test conditions.

Acknowledgments

The authors thank J.W. Geus and H. Meeldijk for the TEM studies, V. Koot for the TPR and H_2 chemisorption measurements, and A.J.M. Mens for the XPS measurements. Financial support was provided by Shell Global Solutions.

References

[1] E. Iglesia, S.L. Soled, J.E. Baumgartner, S.C. Reyes, Top. Catal. 2 (1995) 17.
[2] D. Schanke, S. Vada, E.A. Blekkan, A.M. Hilmen, A. Hoff, A. Holmen, J. Catal. 156 (1995) 85.
[3] A. Kogelbauer, J.G. Goodwin, R. Oukaci, J. Catal. 160 (1996) 125.
[4] G. Jacobs, T.K. Das, Y.Q. Zhang, J.L. Li, G. Racoillet, B.H. Davis, Appl. Catal. A 233 (2002) 263.
[5] A. Guerrero-Ruiz, A. Sepulveda-Escribano, I. Rodriguez-Ramos, Appl. Catal. A 120 (1994) 71.
[6] G.J. Haddad, B. Chen, J.G. Goodwin, J. Catal. 161 (1996) 274.
[7] G.R. Moradi, M.M. Basir, A. Taeb, A. Kiennemann, Catal. Commun. 4 (2003) 27.
[8] M. van der Riet, G.J. Hutchings, R.G. Copperthwaite, J. Chem. Soc., Chem. Commun. (1986) 798.
[9] K. Guse, H. Papp, Fresenius J. Anal. Chem. 346 (1993) 84.
[10] M.J. Keyser, R.C. Everson, R.L. Espinoza, Appl. Catal. A 171 (1998) 99.
[11] S.E. Colley, R.G. Copperthwaite, G.J. Hutchings, S.P. Terblanche, M.M. Thackeray, Nature 339 (1989) 129.
[12] S. Colley, R.G. Copperthwaite, G.J. Hutchings, M. Van der Riet, Ind. Eng. Chem. Res. 27 (1988) 1339.
[13] F. Morales, F.M.F. de Groot, P. Glatzel, E. Kleimenov, H. Bluhm, M. Havecker, A. Knop-Gericke, B.M. Weckhuysen, J. Phys. Chem. B 108 (2004) 16201.
[14] F.M. Cano, O.L.J. Gijzeman, F.M.F. de Groot, B.M. Weckhuysen, Stud. Surf. Sci. Catal. 147 (2004) 271.
[15] Y.-Q. Zhang, B. Zhong, Q. Wang, J. Nat. Gas Chem. 6 (1997) 275.
[16] M. Johns, P. Landon, T. Alderson, G.J. Hutchings, Chem. Commun. (2001) 2454.
[17] J.J.C. Geerlings, M.F. Goes, H.M. Huisman, J.-P. Lange, H. Oosterbeek, P.J.M. Rek, D. Schadenhorst, WO Patent 9700231 (1997), to Royal Dutch Shell.
[18] M. Jiang, N. Koizumi, T. Ozaki, M. Yamada, Appl. Catal. A 209 (2001) 59.
[19] F. Morales, D. Grandjean, F.M.F. de Groot, O. Stephan, B.M. Weckhuysen, Phys. Chem. Chem. Phys. 7 (2005) 568.
[20] F. Morales, F.M.F. de Groot, O.L.J. Gijzeman, A. Mens, O. Stephan, B.M. Weckhuysen, J. Catal. 230 (2005) 301.
[21] K.P. de Jong, J.W. Geus, Catal. Rev.-Sci. Eng. 42 (2000) 481.
[22] G.L. Bezemer, A. van Laak, A.J. van Dillen, K.P. de Jong, Stud. Surf. Sci. Catal. (2004) 259.
[23] G.L. Bezemer, U. Falke, A.J. van Dillen, K.P. de Jong, Chem. Commun. (2005) 701.
[24] M.L. Toebes, J.H. Bitter, A.J. van Dillen, K.P. de Jong, Catal. Today 76 (2002) 33.
[25] M.L. Toebes, E.M.P. van Heeswijk, J.H. Bitter, A.J. van Dillen, K.P. de Jong, Carbon 42 (2004) 307.
[26] H.P.C.E. Kuipers, Solid State Ionics 16 (1985) 15.
[27] H.P.C.E. Kuipers, H.C.E. Van Leuven, W.M. Visser, Surf. Interface Anal. 8 (1986) 235.
[28] F. Winter, G.L. Bezemer, C. van der Spek, J.D. Meeldijk, A.J. van Dillen, J.W. Geus, K.P. de Jong, Carbon 43 (2005) 327.
[29] R.C. Reuel, C.H. Bartholomew, J. Catal. 85 (1984) 63.
[30] V. Dureuil, C. Ricolleau, M. Gandais, C. Grigis, Eur. Phys. J. D 14 (2001) 83.
[31] M. Oku, K. Hirokawa, J. Electron. Spectrosc. Relat. Phenom. 8 (1976) 475.
[32] M.A. Langell, F. Gevrey, M.W. Nydegger, Appl. Surf. Sci. 153 (2000) 114.
[33] C.J. Bertole, C.A. Mims, G. Kiss, J. Catal. 221 (2004) 191.
[34] E. Iglesia, Appl. Catal. A 161 (1997) 59.
[35] M.E. Levin, K.J. Williams, M. Salmeron, A.T. Bell, G.A. Somorjai, Surf. Sci. 195 (1988) 341.
[36] M.E. Levin, M. Salmeron, A.T. Bell, G.A. Somorjai, J. Catal. 106 (1987) 401.
[37] E. Iglesia, S.L. Soled, R.A. Fiato, G.H. Via, Stud. Surf. Sci. Catal. 81 (1994) 433.
[38] C.J. Bertole, C.A. Mims, G. Kiss, J. Catal. 210 (2002) 84.
[39] J.L. Martin de Vidales, E. Vila, R.M. Rojas, O. Garcia-Martinez, Chem. Mater. 7 (1995) 1716.